Chinese Chemical Letters 35 (2024) 108658

Contents lists available at ScienceDirect

Chinese Chemical Letters

journal homepage: www.elsevier.com/locate/cclet

Evaluation of erastin synergized cisplatin anti-nasopharyngeal carcinoma effect with a glutathione-activated near-infrared fluorescent probe

Rong He[a,b,c], Dandan Tang[b], Ningge Xu[b], Heng Liu[a,b,*], Kun Dou[a,b], Xuejun Zhou[a,b,*], Fabiao Yu[a,b,*]

[a] Department of Otolaryngology, Head and Neck Surgery, The First Affiliated Hospital of Hainan Medical University, Haikou 570102, China
[b] Key Laboratory of Hainan Trauma and Disaster Rescue, Key Laboratory of Emergency and Trauma, Ministry of Education, Engineering Research Center for Hainan Bio-Smart Materials and Bio-Medical Devices, College of Emergency and Trauma, Hainan Medical University, Haikou 571199, China
[c] Sichuan Provincial General Hospital of Judicial Police, Chengdu 610225, China

ARTICLE INFO

Article history:
Received 13 April 2023
Revised 2 June 2023
Accepted 6 June 2023
Available online 7 June 2023

Keywords:
Glutathione
NIRF probe
Ferroptosis
Anti-tumor therapy evaluation
Bioimaging

ABSTRACT

Nasopharyngeal carcinoma (NPC), a malignant tumor originating from the nasopharynx, is one of the common malignant tumors of the head and neck. There are significant geographical differences in the incidence of nasopharyngeal carcinoma, with a high incidence in China and Southeast Asian countries. Herein, we designed and synthesized a novel near-infrared fluorescent (NIRF) probe to detect glutathione (GSH) in cellular and tumor environments using semi-naphthofluorescein (SNAFL) as the fluorescent molecular backbone and 2-fluoro-4-nitrobenzenesulfonate as the recognition moiety. Upon reaction with GSH, SNAFL-GSH emitted a fluorescence signal, and its emission wavelength at 650 nm was remarkably enhanced. The results of selectivity experiments indicated that SNAFL-GSH was able to discriminate GSH from Cys, Hcy, and H_2S. Moreover, SNAFL-GSH could image both endogenous and exogenous GSH and distinguish normal and cancer cells by fluorescence signal difference. At the cellular level, cisplatin (DDP)-induced ferroptosis and inhibition of proliferation of various NPC cell lines (CNE2, CNE1, 5–8F cells) by erastin combined with DDP were visualized with the help of SNAFL-GSH. In a mouse tumor xenograft model, we successfully employed SNAFL-GSH for the evaluation of the efficacy of erastin combined with DDP in the treatment of NPC. More importantly, the probe could image cancerous tissue sections from NPC patients with an imaging depth of approximately 80 μm. It was foreseen that SNAFL-GSH offered great potential for application in the diagnosis and evaluation of the therapeutic efficacy of NPC, and these results would also provide new ideas for the clinical treatment of NPC.

Glutathione (GSH), a tripeptide molecule composed of glutamate, cysteine, and glycine, is the most abundant non-protein thiol in cells [1]. In living organisms, GSH plays essential physiological roles, such as immunity regulation, redox homeostasis modulation, and signaling pathways [2]. Generally speaking, GSH levels are higher in tumor cells than in normal cells. The explanation for this is that tumor cells upregulate glutathione levels to maintain their survival and proliferation in response to rapid metabolic demands and oxidative stress in the microenvironment [3,4]. Nasopharyngeal carcinoma (NPC) is a malignant tumor that occurs in the top and side walls of the nasopharyngeal cavity, which is mainly treated with radiotherapy and chemotherapy in clinical practice [5–7]. Despite its significant side effects, cisplatin (DDP), a traditional chemotherapy regimen, still occupies an important place in NPC chemotherapy. DDP is used to inhibit cancer cell appreciation and induce programmed apoptosis by binding to specific DNA and affecting the DNA replication of cancer cells. It has been found that long-term use of this drug leads to resistance in humans, and the mechanism of DDP resistance is related to its altered transport and metabolism, enhanced DNA repair or tolerance, and blocked apoptosis of cells [8–10]. Importantly, GSH may also be closely implicated with DDP resistance. Once DDP is taken up by cells, GSH can bind to DDP so that it stays in the cytoplasm and does not enter the nucleus to interact with target DNA, ultimately leading to DDP resistance. Commonly administered chemotherapeutic agents such as DDP can reduce the toxic effects on cells

* Corresponding authors.
E-mail addresses: liuheng@hainmc.edu.cn (H. Liu), xuejunzhouent@hainmc.edu.cn (X. Zhou), yufabiao@hainmc.edu.cn (F. Yu).

https://doi.org/10.1016/j.cclet.2023.108658
1001-8417/

by binding to intracellular GSH and converting it into excretable metabolites, a process catalyzed by glutathione *S*-transferase [11]. Nevertheless, prolonged DDP treatment also leads to increased levels of intracellular oxidative stress and decreased GSH levels. Ferroptosis is a novel form of apoptosis that occurs with lipid peroxide accumulation and decreased glutathione peroxidase 4 and GSH levels [12,13]. It has been shown that ferroptosis inducers erastin enhance the sensitivity of tumor cells to chemotherapeutic agents [14–16]. Consequently, the development of analytical methods to dynamically monitor the variation of GSH levels during the treatment of tumors with erastin synergized DDP is critical for understanding its mechanism of action.

Numerous techniques have been employed to measure GSH in biological samples, including Raman spectroscopy, high-performance liquid chromatography (HPLC), mass spectrometry, *etc*. [17,18]. These analytical methods are not well-suited for real-time detection of GSH in live cells and *in vivo* due to the complex pre-treatment and long analysis time required. In order to improve the comprehension of GSH, there is a need to develop strategies capable of monitoring GSH in biosystems. Until now, considerable efforts have been devoted to the development of effective fluorescent probes for tracking GSH in biosystems [19–22]. In light of the sensing mechanism, GSH fluorescent probes involve S-O bond cleavage [23–25], nucleophilic aromatic substitution [26–31], Michael addition [32–34], disulfide bond cleavage [35], and so on [36–40]. Some of these reported probes are still limited by long response times and poor selectivity, which makes it still challenging to design fluorescent probes with high specificity and rapid response to GSH. Furthermore, there are no available fluorescent probes for dynamic visual monitoring of the efficacy of erastin synergistic DDP for NPC treatment.

In this contribution, we fabricated a highly selective near-infrared fluorescent (NIRF) probe for GSH detection and *in vivo* imaging based on a semi-naphthofluorescein (SNAFL) fluorophore. Because the hydroxyl group of the SNAFL fluorophore was masked by the electron-withdrawing group 2-fluoro-4-nitrobenzenesulfonyl, making its intramolecular charge transfer (ICT) hindered, SNAFL-GSH barely fluoresces in the absence of GSH. The addition of GSH triggered the release of the fluorophore, causing a strong fluorescent signal. Using this probe, we monitored changes in GSH levels in cells and tumor-bearing mice. The results showed that DDP induces ferroptosis in cancer cells, while erastin enhanced the therapeutic effect of DDP on tumor-bearing mice.

It is well known that fluorescent probes emitting light in the near-infrared (NIR) range (650–900 nm) are more desirable for *in vivo* imaging [41–46]. SNAFL fluorophores featured high fluorescence quantum efficiency, photostability, and excellent cell permeability and were often employed in the design of fluorescent probes [47,48]. By attaching 2-fluoro-4-nitrobenzenesulfonyl chloride to the SNAFL fluorophore, we synthesized the NIR fluorescent probe SNAFL-GSH. Compared to the previously widely reported 2,4-dinitrobenzenesulfonate, 2-fluoro-4-nitrobenzenesulfonate exhibited higher selectivity for GSH [49–52]. As presented in Figs. 1a and b, the electron-withdrawing group 2-fluoro-4-nitrobenzene sulfonyl effectively inhibited ICT in the structure of SNAFL and quenches the fluorescence emission of SNAFL-GSH. In the presence of GSH, GSH nucleophilically attacked the 2-fluoro-4-nitrophenyl group and triggered intense NIR fluorescence emission by specifically cleaving the C-S bond to restore the push-pull electron system in SNAFL. In addition, recording the change in fluorescence intensity of SNAFL-GSH at 650 nm allowed the quantification of GSH. To verify the reaction mechanism of SNAFL-GSH with GSH, mass spectrum was performed. As seen in Figs. S6 and S7 (Supporting information), the reaction of SNAFL-GSH with excess GSH resulted in the observation of the major molecular ion peak at 437.1643, which was attributed to SNAFL. The chemical structure of SNAFL and SNAFL-GSH was confirmed by nuclear magnetic resonance (^{1}H NMR, ^{13}C NMR), high resolution mass spectroscopy (HRMS), and the characterization profiles were provided in the Supporting information (Figs. S1–S5 in Supporting information).

In initial studies, normalized excitation and fluorescence emission spectra of SNAFL-GSH in the presence of GSH were recorded (Fig. 1c). The optimal excitation and fluorescence emission wavelengths for SNAFL-GSH were determined to be 589 nm and 650 nm, respectively. Fig. S8 (Supporting information) also showed that a strong absorption peak at 589 nm emerged in the presence of GSH. Then 560 nm was chosen as the excitation wavelength for the spectroscopic tests. SNAFL-GSH was originally non-fluorescent due to the ring-closed form of semi-naphthofluorescein. The addition of GSH at concentrations ranging from 0 to 1 mmol/L produced gradually enhanced fluorescence at 650 nm (Fig. 1d), and the fluorescence intensity of SNAFL-GSH at 650 nm exhibited a satisfactory linear relationship with the concentration of GSH between 0.02 mmol/L and 0.4 mmol/L (linear equation $F_{650\ \mathrm{nm}}/10^4 = 528.1x + 1.646$). Using the calculated equation $3\sigma/k$ (where k represents the slope of the linear equation and σ represents the standard deviation of 10 consecutive determinations of the blank sample), the detection limit for GSH was found to be 1.27 μmol/L (Fig. 1e). As can be seen from Fig. S9 (Supporting information), SNAFL-GSH remained stable for 20 min. The fluorescence intensity of SNAFL-GSH in the presence of GSH showed an increasing trend with prolongation of the response time and reached saturation within 15 min, which implied that the ideal reaction time of SNAFL-GSH with GSH was 15 min (Fig. 1f, Fig. S9). The effect of pH on the fluorescence intensity was displayed in Fig. 1g. The fluorescence intensity of SNAFL-GSH was essentially stable in the pH range of 3.0–9.0 and increased at greater than 9.0 due to the alkaline environment-induced semi-naphthofluorescein ring opening. In the presence of GSH, SNAFL-GSH presented a significant fluorescence response in the pH range of 6.0–11.0, indicating its suitability for the detection of GSH in the physiological pH range. To confirm selectivity, the fluorescence response to SNAFL-GSH was examined using common physiologically reactive species, such as amino acids (Lys, Gly, Met, Trp, Pro, Leu, Ser, Val, Arg), anions (HSO_3^-, SO_4^{2-}, CO_3^{2-}, NO_3^-), cations (K^+, Na^+, Mg^{2+}, Zn^{2+}), reactive oxygen species (H_2O_2, ClO^-), reactive sulfur species (GSSG, H_2S, Hcy, Cys) as interferents (Fig. 1h). Of these, Hcy and Cys-induced slight changes in the fluorescence of SNAFL-GSH, whereas all other species gave no fluorescence response. Only the addition of GSH triggered an intense NIR fluorescence of SNAFL-GSH. These results suggested SNAFL-GSH could meet the sensitivity and selectivity requirements for the detection of GSH in biosystems.

Prior to carrying out bioimaging applications, four different cell lines, human normal nasopharyngeal cell line (NP69), human poorly differentiated nasopharyngeal carcinoma cell line (CNE2), human highly differentiated nasopharyngeal carcinoma cell line (CNE1), and human high metastatic nasopharyngeal carcinoma cell line (5–8F) were selected for cytotoxicity evaluation of SNAFL-GSH (Fig. S10 in Supporting information). The cell viability of four cell lines showed a decrease as the concentration of SNAFL-GSH went from 0 to 60 μmol/L. However, the survival rate of all four cell lines was above 80% at the concentration of 60 μmol/L, which illustrated SNAFL-GSH had good biocompatibility and could be employed for the subsequent bioimaging experiments. We first investigated the optimized time for SNAFL-GSH to image GSH at the cellular level (Figs. S11 and S14 in Supporting information). By recording real-time imaging images of SNAFL-GSH incubated with CNE1 cells at different time points (5, 10, 15, 20, 40, 60 min), it was found that

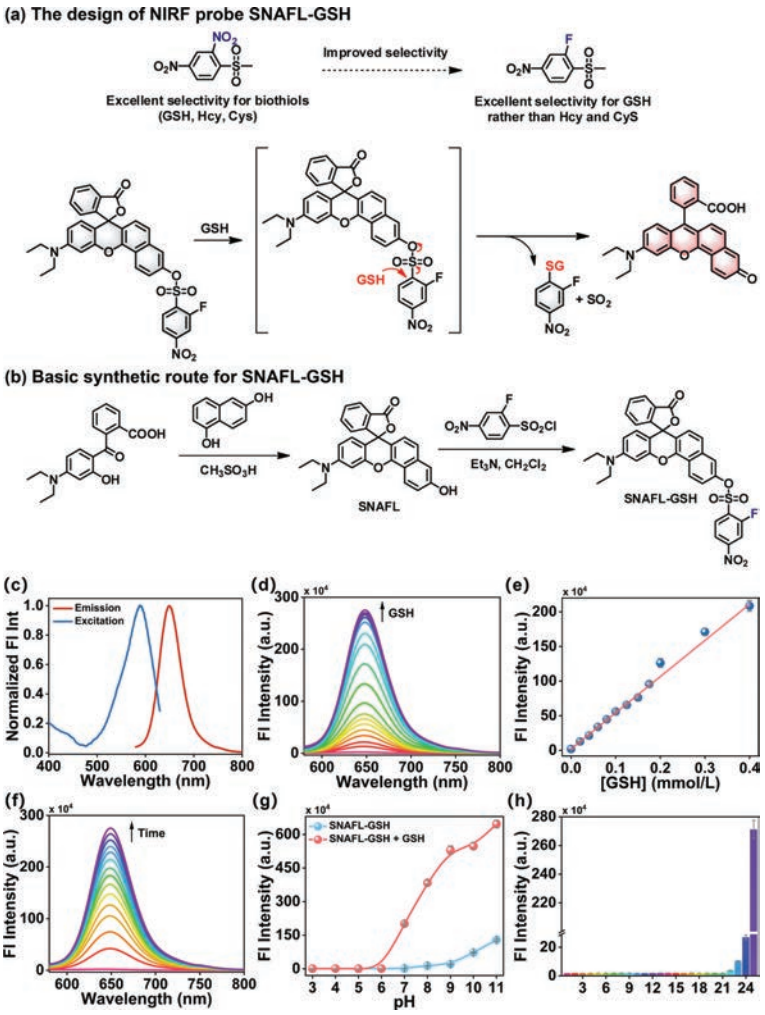

Fig. 1. (a) The design of NIRF probe SNAFL-GSH. (b) Basic synthetic route for SNAFL-GSH. (c) Normalized excitation and fluorescence emission spectra of SNAFL-GSH (10 μmol/L) in the presence of GSH (1 mmol/L). (d) The fluorescence spectra of SNAFL-GSH (10 μmol/L) with the treatment of varied levels of GSH (0–1 mmol/L). (e) Linear fitting curve of fluorescence intensities at 650 nm against GSH concentration from 0 to 0.4 mmol/L. (f) The fluorescence spectra of SNAFL-GSH with the addition of GSH (1 mmol/L) for various time from 0 min to 20 min. (g) Fluorescence intensities at 650 nm of SNAFL-GSH in the absence or presence of GSH (1 mmol/L) under different pH values (3.0–11.0). (h) Fluorescence intensities at 650 nm of SNAFL-GSH upon the treatment of different analytes. From 1 to 24: blank, Lys (1 mmol/L), Gly (1 mmol/L), Met (1 mmol/L), Trp (1 mmol/L), Pro (1 mmol/L), Leu (1 mmol/L), Ser (1 mmol/L), Val (1 mmol/L), Arg (1 mmol/L), HSO_3^- (100 μmol/L), SO_4^{2-} (100 μmol/L), CO_3^{2-} (100 μmol/L), NO_3^- (100 μmol/L), K^+ (100 μmol/L), Na^+ (100 μmol/L), Mg^{2+} (100 μmol/L), Zn^{2+} (100 μmol/L), H_2O_2 (100 μmol/L), ClO^- (100 μmol/L), GSSG (1 mmol/L), H_2S (50 μmol/L), Hcy (50 μmol/L), Cys (200 μmol/L), GSH (1 mmol/L). The data were shown as mean ± standard deviation (s.d.) (n = 3). λ_{ex} = 560 nm, λ_{em} = 580–800 nm.

the red fluorescence signal reached a maximum at 20 min, followed by a stepwise decrease within 60 min. So, the incubation time of SNAFL-GSH with cells in the follow-up biological experiments was set at 20 min. The capability of SNAFL-GSH to image GSH in different human nasopharyngeal cell lines was examined (Figs. S12 and S15 in Supporting information). After incubating SNAFL-GSH with NP69, CNE2, CNE1, and 5–8F cells for 20 min and then imaging, it was observed that the red fluorescence signal in CNE2, CNE1, and 5–8F cells was apparently higher than that in NP69 cells, which meant GSH was expressed at a higher level in cancer cells than in normal cells. The above experimental results demonstrated that SNAFL-GSH could be exploited for the differentiation of cancer cells from normal cells.

Subsequently, NIRF imaging of endogenous GSH in three NPC cell lines (CNE2, CNE1, 5–8F cells) was carried out. As presented in Figs. 2a and b, all three different NPC cell lines incubated with SNAFL-GSH produced a robust red fluorescent signal. When the cells were treated with *N*-ethylmaleimide (NEM, a well-known thiol-blocking reagent) for 30 min and then incubated with SNAFL-GSH for 20 min, the red fluorescence signal was markedly suppressed. As NEM-treated cells were incubated sequentially with glutathione reduced ethyl ester (GSH–OEt) and SNAFL-GSH, the red fluorescence signal in cells was restored, demonstrating SNAFL-GSH was able to image endogenous GSH in various cancer cell lines. Previous studies have demonstrated that DDP could lead to a decrease in GPX activity and GSH levels in cancer cells, which were closely related to ferroptosis [53]. To verify whether DDP could induce ferroptosis, we conducted the following cell imaging experiments. As indicated in Figs. 2c and d, a pronounced decrease in intracellular red fluorescence signal relative to the control group was observed in three cancer cells (CNE2, CNE1, 5–8F cells) treated with DDP for 24 h. Ferrostatin-1 (Fer-1) was a compound with ferroptosis inhibitory effects that inhibited iron-dependent cancer cell death by blocking cystine transport and glutathione production. Compared with cells treated with DDP alone, the red fluorescence signal in cells co-cultured with DDP and Fer-1 was recovered to varying degrees. The results suggested that DDP might promote cancer cell death through ferroptosis, and Fer-1 could suppress iron-dependent cell death and GSH depletion.

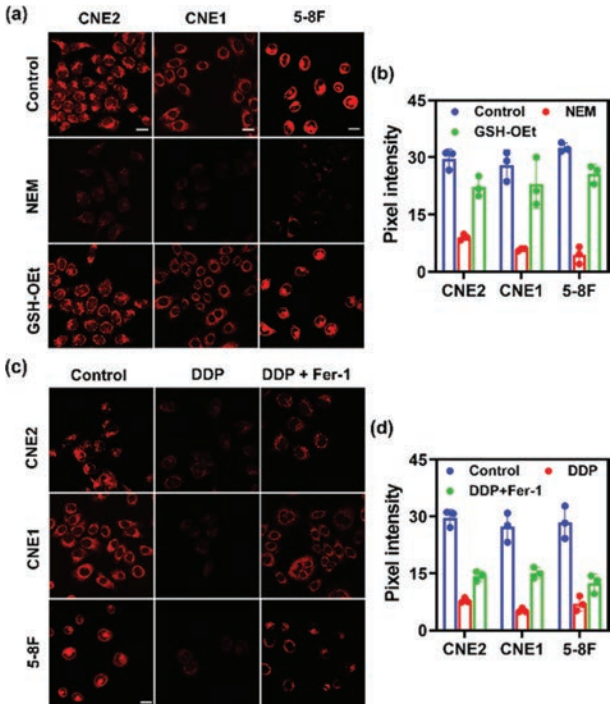

Fig. 2. Fluorescence images of GSH in various NPC cell lines (CNE2, CNE1, 5–8F cells). (a) Control group: fluorescence imaging of GSH in CNE2, CNE1, 5–8F cells with the addition of SNAFL-GSH (10 μmol/L) for 20 min; NEM group: fluorescence imaging of GSH in CNE2, CNE1, 5–8F cells with the sequential addition of NEM (1 mmol/L) and SNAFL-GSH (10 μmol/L); GSH–OEt group: fluorescence imaging of GSH in CNE2, CNE1, 5–8F cells with the sequential addition of NEM (1 mmol/L), GSH–OEt (1 mmol/L) and SNAFL-GSH (10 μmol/L). Scale bar: 20 μm. (b) Pixel intensity of images in (a). The data were shown as mean ± s.d. (n = 3). Fluorescence images of GSH in various cell lines (CNE2, CNE1, 5–8F cells) during DDP-induced ferroptosis. (c) Control group: fluorescence imaging of GSH in CNE2, CNE1, 5–8F cells with the addition of SNAFL-GSH (10 μmol/L) for 20 min; DDP group: fluorescence imaging of GSH in CNE2, CNE1, 5–8F cells with the sequential addition of DDP (20 μmol/L, 24 h) and SNAFL-GSH (10 μmol/L); DDP/Fer-1 group: fluorescence imaging of GSH in CNE2, CNE1, 5–8F cells with the sequential addition of DDP (20 μmol/L) plus Fer-1 (5 μmol/L), and SNAFL-GSH (10 μmol/L). Scale bar: 20 μm. (d) Pixel intensity of images in (c). The data were shown as mean ± s.d. (n = 3). λ_{ex} = 561 nm; red channel: λ_{em} = 600–700 nm.

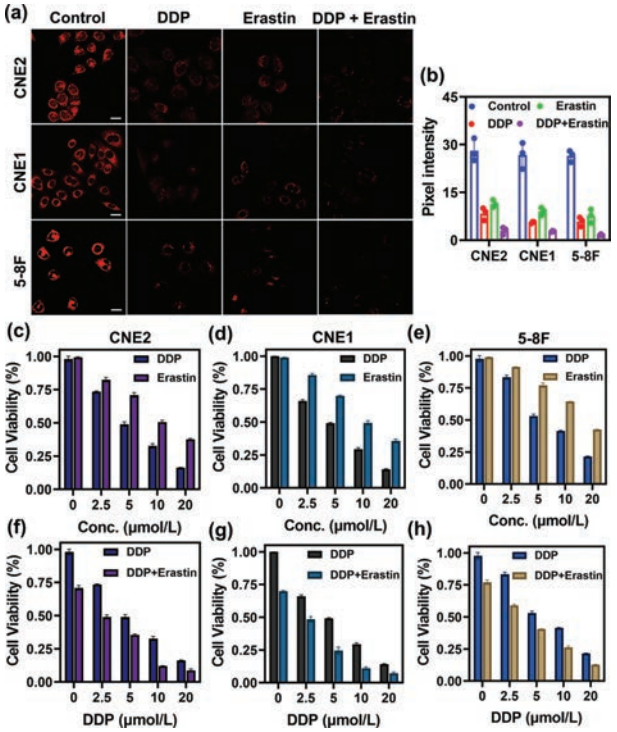

Fig. 3. Fluorescence images of GSH in various cell lines (CNE2, CNE1, 5–8F cells) under different drug treatments (DDP, erastin, DDP plus erastin). (a) Control group: fluorescence imaging of GSH in CNE2, CNE1, 5–8F cells with the addition of SNAFL-GSH (10 μmol/L) for 20 min; DDP group: fluorescence imaging of GSH in CNE2, CNE1, 5–8F cells with the sequential addition of DDP (20 μmol/L, 24 h) and SNAFL-GSH (10 μmol/L); Erastin group: fluorescence imaging of GSH in CNE2, CNE1, 5–8F cells with the sequential addition of erastin (5 μmol/L) and SNAFL-GSH (10 μmol/L); DDP/Erastin group: fluorescence imaging of GSH in CNE2, CNE1, 5–8F cells with the sequential addition of DDP (20 μmol/L) plus erastin (5 μmol/L), and SNAFL-GSH (10 μmol/L). Scale bar: 20 μm. (b) Pixel intensity of images in (a). The data were shown as mean ± s.d. (n = 3). λ_{ex} = 561 nm; red channel: λ_{em} = 600–700 nm. Erastin synergizes with DDP to increase cytotoxicity to various nasopharyngeal carcinoma cells (CNE2, CNE1, 5–8F cells). (c–e) CNE2, CNE1, 5–8F cells were treated with different concentrations (0, 2.5, 5, 10, 20 μmol/L) of DDP or erastin for 24 h, respectively. (f–h) CNE2, CNE1, and 5–8F cells were treated with different concentrations (0, 2.5, 5, 10, 20 μmol/L) of DDP in the presence of erastin (5 μmol/L). The data were shown as mean ± s.d. (n = 3).

Using SNAFL-GSH, we further investigated the changes in intracellular GSH levels in the three NPC cells treated with different drugs (DDP, erastin, DDP plus erastin). Fig. 3a depicted that the red fluorescence signal was intense in the control group, while the red fluorescence intensity in cells treated with DDP or erastin alone was reduced to different degrees, and the red fluorescence intensity in DDP-treated cells was greater than in erastin-treated cells. The red fluorescence intensity in the cells treated with DDP combined with erastin was reduced more than that in the cells treated with DDP or erastin alone (Fig. 3b). This indicated that the GSH concentration in the cells treated with DDP combined with erastin was significantly lower than that in the cells treated with DDP or erastin alone. In addition, the toxicity of different drug treatments on three types of cancer cells was also evaluated. In the DDP or erastin-treated group, cell viability decreased gradually with increasing concentrations of DDP and erastin (Figs. 3c–e). The half maximal inhibitory concentration (IC_{50}) values of DDP on CNE2, CNE1, and 5–8F cells were (4.83 ± 0.49), (4.83 ± 0.19), and (5.37 ± 0.19) μmol/L, while those of erastin were (9.75 ± 2.37), (9.53 ± 2.46), and (11.27 ± 3.38) μmol/L. When CNE2, CNE1, and 5–8F cells were treated with different concentrations of DDP (0, 2.5, 5, 10, 20 μmol/L) in the presence of erastin (5 μmol/L), cell viability was dramatically lower than that of the DDP-treated group (Figs. 3f–h). The IC_{50} values of DDP combined with erastin were calculated to be (2.52 ± 0.42), (2.27 ± 0.05), and (3.62 ± 0.81) μmol/L. These data illustrated that DDP synergized with erastin increased the cytotoxicity of cancer cells with maximum antitumor effect, while SNAFL-GSH allowed visual monitoring of this process by variations in GSH levels.

Motivated by the outstanding performance of SNAFL-GSH for optical imaging at the cellular level, we next explored whether it could be used for monitoring DDP in combination with erastin for the treatment of tumors in mice [54,55]. All experimental protocols were approved by the Institutional Animal Care and Use Committee of Hainan Medical University (Haikou, China). 5–8F xenograft tumor models were established in nude mice. The tumor-bearing mice were divided into three groups. These three groups were injected intraperitoneally with erastin, DDP, erastin plus DDP every other day for two weeks, respectively. As shown in Fig. 4, the mice showed little change in fluorescence after erastin treatment, while the mice before and after DDP treatment displayed a noticeable change in fluorescence. The decrease in fluorescence was obviously greater in erastin combined with DDP-treated mice compared to DDP-treated mice. These findings suggested that erastin might synergistically treat tumors by increasing the sensitivity of cancer cells

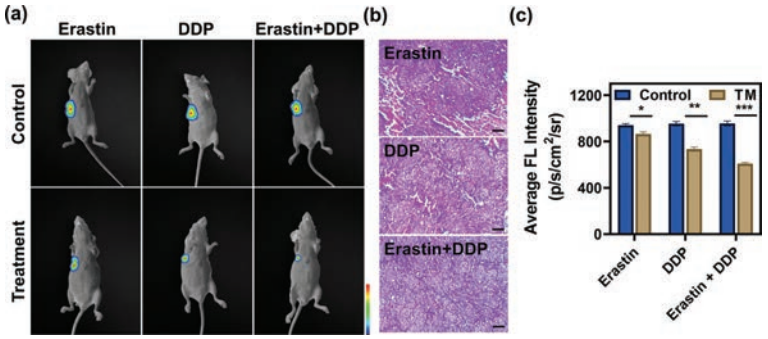

Fig. 4. *In vivo* imaging of GSH levels in the process of different drug treatments. (a) NIRF images of erastin-treatment, DDP-treatment, and erastin plus DDP-treatment groups of 5–8F-tumor-bearing BALB/c mice after intratumoral injection of SNAFL-GSH (50 μmol/L, 50 μL). (b) H&E staining of tumors after erastin, DDP, erastin plus DDP treatment. Scale bar: 200 μm. (c) Quantified average fluorescence intensity in the tumor region. Data were expressed as mean ± s.d. ($n = 3$). Statistical analysis was conducted with multiple *t*-tests ($^{*}P < 0.01$, $^{**}P < 0.001$, $^{***}P < 0.001$).

to DDP and alterations of GSH levels in tumors were positively correlated with the effect of DDP synergized with erastin treatment. The experimental results of hematoxylin-eosin (H&E) staining also further supported the above conclusion.

To discover whether SNAFL-GSH could be utilized for the detection of GSH in human NPC, we took fresh sections of NPC patients for confocal imaging. Fresh sections with a thickness of 80 μmol/L were incubated with SNAFL-GSH for 30 min, washed three times with phosphate buffered saline (PBS), and then imaged. The confocal Z-axis imaging confirmed that SNAFL-GSH enabled imaging of cancerous tissues close to 80 μm in NPC patients (Fig. S13 in Supporting information). The results showed that SNAFL-GSH possessed excellent penetration ability and had the potential for accurate clinical imaging of GSH in NPC tissues.

In summary, we designed and synthesized a novel NIRF probe SNAFL-GSH with exclusive selectivity for GSH. In *in vitro* experiments, SNAFL-GSH itself had almost no fluorescence but showed dramatic fluorescence enhancement in the presence of GSH. The enhanced fluorescence of SNAFL-GSH was generated from the cleavage of 2-fluoro-4-nitro sulfonate to release the fluorophore SNAFL. Given the low cytotoxicity, SNAFL-GSH was exploited for NIRF imaging of GSH in cells and tumor-bearing mice *in vivo*. SNAFL-GSH had the ability to differentiate cancer cells from normal cells and visualize variations in GSH concentration levels during drug erastin, DDP, or erastin plus DDP induction. Moreover, SNAFL-GSH enabled the evaluation of antitumor drugs and imaging of human NPC tissue sections. With the assistance of SNAFL-GSH, we confirmed erastin synergized with DDP was more effective than DDP administration alone in treating tumors. Notably, SNAFL-GSH might be a particularly suitable tool for tracking the tumor treatment process and screening of antitumor drugs.

Declaration of competing interest

The authors declare that they have no known competing financial interests or personal relationships that could have appeared to influence the work reported in this paper.

Acknowledgments

This work was supported by the Hainan Province Science and Technology Special Fund (Nos. ZDYF2021SHFZ219, ZDYF2022SHFZ288), National Natural Science Foundation of China (Nos. 21961010, 22264013, 22204037), Hainan Provincial Natural Science Foundation of China (No. 822RC831), Natural Science Research Talent Project of Hainan Medical University (No. JBGS202101), Hainan Province Clinical Medical Center (2021), and Project for Functional Materials and Molecular Imaging Science Innovation Group of Hainan Medical University. Human nasopharyngeal carcinoma tissues were obtained from Department of Otolaryngology, Head and Neck Surgery, the First Affiliated Hospital of Hainan Medical University.

Supplementary materials

Supplementary material associated with this article can be found, in the online version, at doi:10.1016/j.cclet.2023.108658.

References

[1] J. Sastre, F.V. Pallardo, J. Viña, Glutathione, in: T. Grune (Ed.), Reactions, Processes: Oxidants and Antioxidant Defense Systems, Springer Berlin Heidelberg, Berlin, Heidelberg, 2005, pp. 91–108.
[2] G. Teskey, R. Abrahem, R. Cao, et al., Glutathione as a marker for human disease, in: G.S. Makowski (Ed.), Advances in Clinical Chemistry, Elsevier, London, 2018, pp. 141–159.
[3] G.K. Balendiran, R. Dabur, D. Fraser, Cell Biochem. Funct. 22 (2004) 343–352.
[4] M.P. Gamcsik, M.S. Kasibhatla, S.D. Teeter, et al., Biomarkers 17 (2012) 671–691.
[5] Y. Sun, W.F. Li, N.Y. Chen, et al., Lancet Oncol. 17 (2016) 1509–1520.
[6] Y.P. Chen, A.T.C. Chan, Q.T. Le, et al., Lancet 394 (2019) 64–80.
[7] S. Guan, J. Wei, L. Huang, L. Wu, Eur. J. Med. Chem. 207 (2020) 112758.
[8] M.A. Fuertes, C. Alonso, J.M. Pérez, Chem. Rev. 103 (2003) 645–662.
[9] J.W. Lv, Z.Y. Qi, G.Q. Zhou, et al., Cancer Sci. 109 (2018) 751–763.
[10] M. Song, M. Cui, K. Liu, Eur. J. Med. Chem. 232 (2022) 114205.
[11] T. Jin, W.F. Qin, F. Jiang, et al., Transl. Oncol. 12 (2019) 633–639.
[12] H. Yu, P. Guo, X. Xie, et al., J. Cell. Mol. Med. 21 (2017) 648–657.
[13] J. Li, F. Cao, H.L. Yin, et al., Cell. Death Dis. 11 (2020) 88.
[14] B. Lu, X.B. Chen, M.D. Ying, et al., Front. Pharmacol. 8 (2017) 992.
[15] X. Xia, X. Fan, M. Zhao, P. Zhu, Curr. Gene Ther. 19 (2019) 117–124.
[16] Y. Zhao, Y. Li, R. Zhang, et al., Onco Targets Ther. 13 (2020) 5429–5441.
[17] D. Giustarini, I. Dalle-Donne, A. Milzani, et al., Nat. Protoc. 8 (2013) 1660–1669.
[18] Y. Zhu, J. Wu, K. Wang, J. Xie, et al., Talanta 224 (2021) 121852.
[19] D. Sun, Z. Chen, J. Hu, et al., Chin. Chem. Lett. 33 (2022) 4478–4494.
[20] D. Chen, Y. Feng, Crit. Rev. Anal. Chem. 52 (2022) 649–666.
[21] Z. Xu, T. Qin, X. Zhou, et al., Trends Anal. Chem. 121 (2019) 115672.
[22] S. Lee, J. Li, X. Zhou, et al., Coord. Chem. Rev. 366 (2018) 29–68.
[23] Y. Zhang, J. Zhang, M. Su, C. Li, Biosens. Bioelectron. 175 (2021) 112866.
[24] F. Liang, S. Jiao, D. Jin, et al., Spectrochim. Acta A 224 (2020) 117403.
[25] Z. Xu, X. Huang, X. Han, et al., Chem 4 (2018) 1609–1628.
[26] N. Li, T. Wang, N. Wang, et al., Angew. Chem. Int. Ed. 62 (2023) e202217326.
[27] W. Shu, J. Yu, H. Wang, et al., Anal. Chim. Acta 1220 (2022) 340081.
[28] W. Liu, J. Chen, Q. Qiao, et al., Chin. Chem. Lett. 33 (2022) 4943–4947.
[29] F. Chen, J. Zhang, W. Qu, et al., Sens. Actuators B: Chem. 266 (2018) 528–533.
[30] K. Umezawa, M. Yoshida, M. Kamiya, et al., Nat. Chem. 9 (2017) 279–286.
[31] D. Gong, S.C. Han, A. Iqbal, et al., Anal. Chem. 89 (2017) 13112–13119.
[32] S. Hou, Y. Wang, Y. Zhang, et al., Anal. Chim. Acta 1214 (2022) 339957.
[33] K. Wang, G. Nie, S. Ran, et al., Dyes Pigments 172 (2020) 107837.
[34] P. Hou, J. Sun, H. Wang, et al., Sens. Actuators B: Chem. 304 (2020) 127244.
[35] Z. Zheng, Y. Huyan, H. Li, et al., Sens. Actuators B: Chem. 301 (2019) 127065.
[36] C. Zhang, Y. Qin, C. Deng, et al., Anal. Chim. Acta 1248 (2023) 340933.
[37] H.M. Jiang, G.X. Yin, Y.B. Gan, et al., Chin. Chem. Lett. 33 (2022) 1609–1612.
[38] X.W. Li, C.Y. Liu, N. Gao, et al., Chin. Chem. Lett. 33 (2022) 2527–2531.
[39] T.X. Jin, M.Y. Cui, D. Wu, et al., Chin. Chem. Lett. 32 (2021) 3899–3902.
[40] Y. Zou, M. Li, Y. Xing, et al., ACS Sens. 5 (2020) 242–249.
[41] N. Ahmed, W. Zareen, Y. Ye, Chin. Chem. Lett. 33 (2022) 2765–2772.
[42] L.R. Jiang, T.H. Chen, E.W. Song, et al., Chem. Eng. J. 427 (2022) 131563.
[43] S.T. Cai, Q.C. Liu, C. Liu, et al., J. Mater. Chem. B 10 (2022) 1265–1271.
[44] S. Xu, W.J. Pan, T.B. Ren, et al., Chin. J. Chem. 40 (2021) 1073–1082.

[45] C. Duan, M. Won, P. Verwilst, et al., Anal. Chem. 91 (2019) 4172–4178.
[46] J.C. Xu, J. Pan, X.M. Jiang, et al., Biosens. Bioelectron. 77 (2016) 725–732.
[47] Y.Y. Ma, Z.C. Xu, Q. Sun, et al., Spectrochim. Acta. A 247 (2021) 1386–1425.
[48] X.Y. Zhang, W.B. Qu, H. L, et al., Anal. Chim. Acta 1109 (2020) 37–43.
[49] J. Dong, G. Lu, Y. Tu, C. Fan, New J. Chem. 46 (2022) 10995–11020.
[50] M.Y. Lucero, J. Chan, Nat. Chem. 13 (2021) 1248–1256.
[51] J. Dai, C. Ma, P. Zhang, et al., Dyes Pigments 177 (2020) 108321.
[52] L.Y. Niu, Y.Z. Chen, H.R. Zheng, et al., Chem. Soc. Rev. 44 (2015) 6143–6160.
[53] J. Hu, W. Gu, N. Ma, et al., Br. J. Pharmacol. 179 (2022) 3991–4009.
[54] Q. Cheng, L. Bao, M. Li, et al., J. Obstet. Gynaecol. Res. 47 (2021) 2481–2491.
[55] M. Sato, R. Kusumi, S. Hamashima, et al., Sci. Rep. 8 (2018) 968.